



Microstructure, Mechanical and Tribological Properties of Al7075/SiC/Graphite Hybrid Metal Matrix Composites

Atla Sridhar^{1,2} · K. Prasanna Lakshmi² · CH. V. Satyanarayana Raju³

Received: 17 March 2022 / Revised: 17 May 2022 / Accepted: 6 June 2022 / Published online: 1 July 2022
© The Author(s), under exclusive licence to Springer Nature Switzerland AG 2022

Abstract

Particulate reinforced aluminium hybrid composites are becoming more popular in automobile, aero and industrial applications. The current work attempts to produce self-lubricating particulates into Al7075–5wt% SiC– x wt% graphite ($x=0, 5,$ and 10) hybrid-composite via the powder metallurgy method. The hybrid composites' density, hardness, microstructural, and tribological properties were studied. The Taguchi experimental design was used to investigate the ideal testing settings utilising an orthogonal array, the signal-to-noise ratio, and analysis of variance. It was observed that reinforcement particles are homogeneously dispersed in the matrix alloy as fine dendrites in aluminium from SEM examination. According to the results. The wear loss increases as the sliding distance and load increase but decreases as the graphite weight percentage increases. Therefore, a confirmation test was also performed with the optimized parameter combinations to validate the Taguchi findings, reducing wear loss by around 45.11% and the friction coefficient by 68.50%. The wear-mechanism has described creating both an adhesive layer and an interfacial layer. The wear mechanisms were explained by examining through SEM and Edax. The wear resistance and friction coefficient of aluminium hybrid composites improved significantly by incorporating a solid lubricant and hard ceramic reinforcing particulate in the matrix alloy.

Keywords Al 7075 · Powder metallurgy · Graphite · Hybrid composites · Tribology properties

1 Introduction

Current engineering applications demand cutting-edge materials featuring customizable mechanical and tribological characteristics to satisfy their practical needs and strengthen the existing metals and alloys [1, 2]. Compared to widely viable metals and alloys, the performance of the aluminium composites reinforced with ceramic particulates is widely known for their outstanding mechanical characteristics, good wear resistance, and superior strength to weight ratio [3–5]. Most manufacturing parts are derived from them

due to their common usage in several industries, including aircraft, automobiles, structures, shipbuilding, naval activities, and electronics [6]. These products are developed systematically for a specific purpose by selecting the appropriate ceramic reinforcing agent and aluminium matrix alloy and employing proven technology, laboratory facilities, and equipment [7, 8]. Over the last two decades, most research has concentrated on exploring the applicability and synchronisation of several ceramic particles as reinforced materials for different aluminium alloy grades and development methods, along with respective microstructural, mechanical, and wear behaviour characteristics [9–14]. To improve specific characteristics, reinforcements are incorporated into the metal matrix. These reinforcements were thus divided into whiskers, particles, fibres, and filaments. The majority of these studies preferred particulate reinforcement over all other types. Particle reinforcements include carbides and oxides, which include Silicon Carbide (SiC), Titanium diboride (TiB₂), Alumina (Al₂O₃), Boron carbide (B₄C), Carbon Fibre, Graphite, Titanium Carbide (TiC) [15]. The exploratory research found that the reinforcement and matrix alloy characteristics used are the initial significant

✉ Atla Sridhar
atla.sridhar9@gmail.com

¹ Department of Mechanical Engineering, GITAM Deemed to Be University Hyderabad, Telangana 502329, India

² Department of Mechanical Engineering, Jawaharlal Nehru Technological University Hyderabad, Telangana 500085, India

³ Control Systems Laboratory, Research Center Imarat, Defence Research and Development Organisation, Hyderabad, Telangana 500069, India

indicators of the composite's characteristics. While Secondary aspects such as the dimensions of the reinforcing ceramic particulates, the manufacturing method, and their controllable parameters are considered [16, 17]. In many investigations, Aluminium composite materials developed with different ceramic particles have been studied in several experiments [18–20]. However, the main disadvantage of ceramic reinforcement materials is secondary abrasive damage to the mating substrate and reduced wear resistance on the aluminium metal matrix composites [21]. Furthermore, adding ceramic particles to an aluminium alloy may increase aluminium composites' hardness and reduce ductility [22].

Moreover, this capacity has increased the difficulty of manufacturing, machining composites and made it more difficult to melt [23, 24]. To overcome these drawbacks, research on various reinforcements must be conducted to understand better their behaviour for a wide range of applications [25, 26]. Al–Gr composites machining study reported a significant decrease in cutting forces. Researchers have hypothesised that this may be due to a reduction in friction from the lubricated solid particles of Graphite [27–29]. Therefore, Gr may be utilized as a secondary reinforcement for softening Ceramic reinforced composites, which has an inherent challenge when machining them [25]. The combination of aluminium alloy, ceramics, and Graphite provides excellent wear characteristics [6, 30]. The In-situ P/M method (IPM) was used to study the impact of Silicon Carbide content on processing, compaction, and attributes of Al 6061/Gr/SiC composites [31, 32]. The literature used a liquid metallurgical method to understand sliding friction in hybrid metal matrix composites (HMMCs), where sliding speeds and subsurface deformation are linked with dry sliding wear [33, 34]. Tribological behaviour, described by the semisolid powder-densification technique of self-lubricative aluminium/SiC/graphite hybrid combination [35, 36]. Aluminium metal matrix composites increased their density, hardness, and wear properties with increased silicon carbide (SiC) weight percentage reinforcement by decreasing ductility and toughness. Graphite is well suited to fixing these types of problems. As a result, very few studies have been conducted on the effects of hard ceramic reinforcements and solid lubricant materials, such as Graphite, fly ash and boron nitride in aluminium alloy hybrid composites [31].

In the past several decades, the properties of particle reinforcements between particles ranging from tens of micrometres to several hundred micrometres in Aluminium metal matrix composites (AMCs) have been extensively investigated [23, 24]. Researchers discovered that reducing the size of reinforcing particles from micron to nano provided more incredible mechanical properties in the composite. Unfortunately, the nanoparticles agglomerate during the metal stir-casting process due to low wettability [37–39]. The aluminium metal matrix composites must be prepared

with an equal distribution of reinforcement particles. Therefore, the biggest challenge involved preparing equally distributed particulates in the composite [21–28]. Processing of composites by powder metallurgy method can overcome this formation of agglomerations and clusters to achieve homogeneous reinforcement particles dispersion in the aluminium matrix [6, 29]. Based on exhaustive literature notes, it was found that the effect of graphite reinforcing materials in the aluminium hybrid composites and processing by powder metallurgy method was rarely documented. Wear properties of AA2024/SiC/Gr hybrid combinations through powder metallurgy route [40]. Very few researchers studied wear properties by the P/M route that limited to the micro-level size of reinforcements, but not at nano levels. A lot of systematic research needs to be done at nano-size by powder metallurgy to understand hybrid combinations on mechanical and tribological behaviour.

The principal objective of this research is to manufacture aluminium hybrid composites composition of Al7075–5wt.% SiC– x wt.% graphite ($x=0, 5, \text{ and } 10$) by powder metallurgy and investigate the mechanical and tribological properties. The Aluminium 7075 alloy matrix was selected because it is one of the strongest aluminium alloys. The material is well-suited for applications like aeroplane and defence components or wear-resistant parts with good strength-to-weight ratios and lower density. Both the mechanical strength and wear resistance of composites increase with the addition of SiC ceramic and graphite particulates to the aluminium matrix alloy. Silicon carbide (SiC) particulates of 25 μm size and Graphite (Gr) particulates of 1 μm size were used as reinforcements.

Moreover, the influence of applied load, sliding velocity, and sliding distance on the wear and friction of the same composites was studied using Taguchi orthogonal array experimentation. The proportion of the effect of different variables and their combinations was determined using ANOVA. Additionally, the SEM micrographs and EDAX of worn-out surfaces were explored to understand the wear mechanisms better.

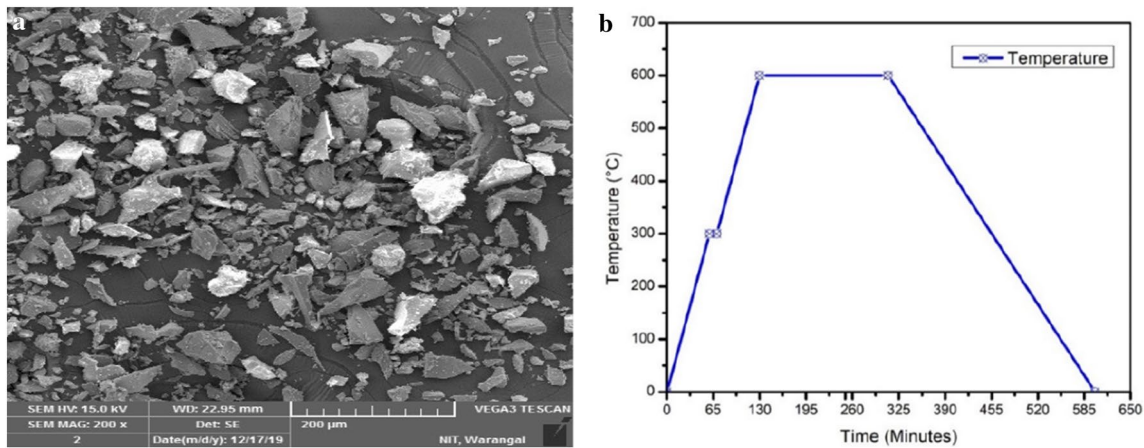
2 Experimentation and Methodology

2.1 Materials

This experiment was performed to prepare Al–SiC–Graphite hybrid composites with powder metallurgical methods to minimize the wear and obtain a single material's superior wear and mechanical properties. Al7075 alloy is a matrix substance, and its chemical composition is specified in Table 1. Silicon carbide (SiC) particulates of 25 μm size and Graphite (Gr) at a 1 μm size were used as reinforcements. The hybrid composites were made with a weight fraction of

Table 1 Chemical components of Al7075 alloy

Components	Si	Fe	Cu	Mn	Mg	Cr	Ni	Zn	Ti	Al
% of composition	0.141	0.193	1.55	0.035	2.24	0.223	0.0075	5.52	0.5	89.95

**Fig. 1** a As received SiC SEM image. b Vacuum sintering process graph

0–10% graphite particles at 5% increments and a constant weight of 5% SiC. The hybrid composites were processed using a powder metallurgy process to ensure uniform dispersion of the reinforcement particles. These metal powders were procured from Prabhu copper Ltd, Mumbai, India. The overall weight of 2000 g of Al 7075 alloy, 1000 g of Silicon carbide (SiC) and 500 g of Graphite (Gr). Figure 1a shows as received SEM image of SiC powder.

2.2 Preparation of Hybrid Composites

Before processing, all powders are preheated in a muffle furnace at 110 °C for 1.25 h to remove moisture. Then, a required composition of Al 7075, SiC and Graphite powders have been processed in a high-energy ball milling using tungsten bowls with 10–50 mm balls and a powder to ball weight ratio of 1:10, with a milling period of up to 60 h. Finally, the blending and exemplary grinding procedures were done at 300 rpm to prevent oxidation or sticking powders on the vial wall using a toluene medium.

The thoroughly blended powders were compressed under a universal testing machine with an applied load of 80 kN at a pressure of 800 MPa. Before every test, zinc stearate (CAS:557-05-1) was used to lubricate the die walls. Then it forms green-compacted samples. Compacted samples were sintered at a temperature of 600 °C in a tube furnace (Kejia model, range 1600 °C) under vacuum conditions. After creating a vacuum in the furnace chamber, the initial temperature heats from 0 to 300 °C for a ramping time of 60 min at an average heating rate of 5 °C/min. Next, they were soaked at a temperature of about 300 °C for 10 min. The next stage

Table 2 Mechanical properties of hybrid-composites

S.No	Reinforcement details (wt.%)	Density (g/cc)	Hardness (HRB)
S-1	Al7075–5%SiC–0% graphite	2.83	77
S-2	Al7075–5%SiC–5% graphite	2.80	73
S-3	Al7075–5%SiC–10% graphite	2.77	68

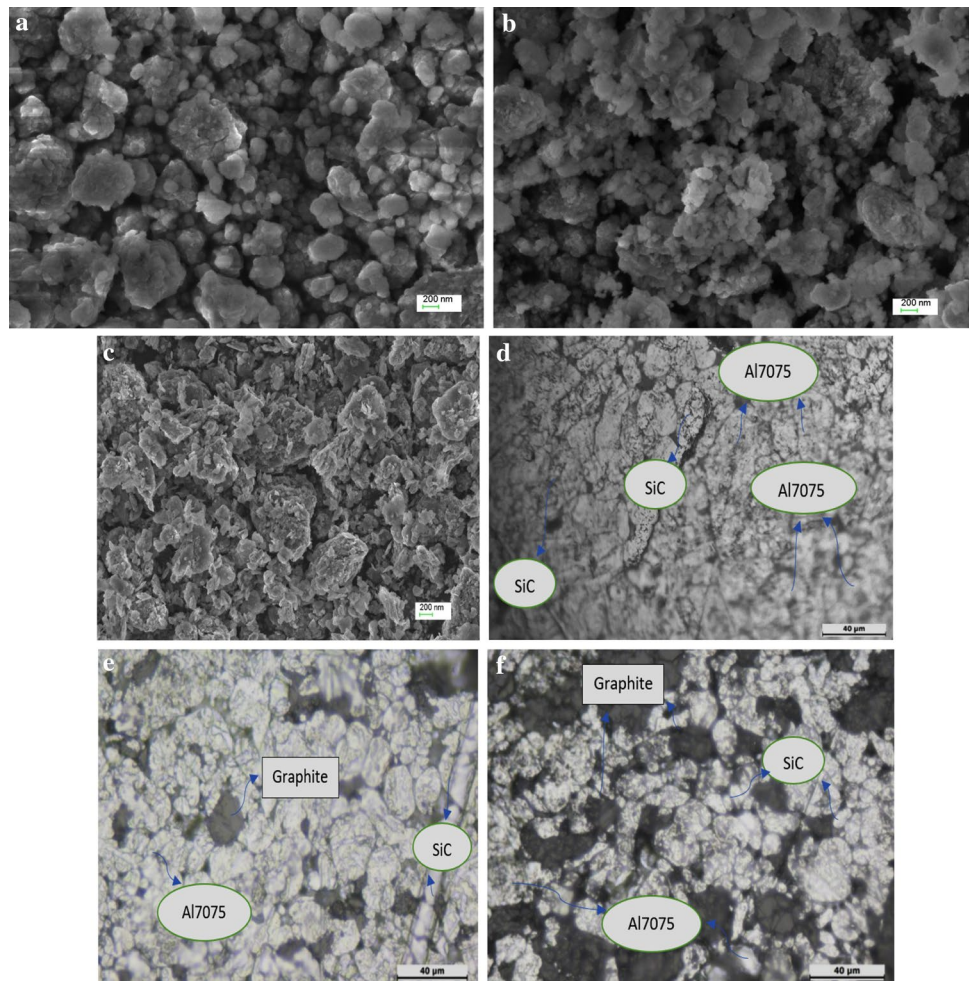
of heating time from 300 to 600 °C is 60 min. Soak it for 180 min at a temperature of 600 °C, then cool it in the same furnace medium till it reaches room temperature. The complete vacuum sintering process is shown in Fig. 1b. Samples are then systematically prepared using different categories of coarse and fine abrasive grit sheets.

2.3 Density and Hardness

The density of the developed hybrid composites was measured using an incredible-precision modern digital weighing machine with an accuracy of 1×10^{-3} mg considering Archimedes' principle. In addition, a Rockwell hardness technique is utilized to measure the hardness of the composite. The mechanical characteristics of the identical specimens are shown in Table 2. By varying Graphite and keeping the SiC constant, the mechanical properties and tribological properties are optimized.

The samples were sectioned and processed according to the principles of metallographic methodology to investigate their microstructural behaviour. Figure 2a–f illustrates the

Fig. 2 a–f Balling and sintering of the hybrid-composites. **a** Al7075-5 wt% SiC -0 wt% Gr after Ball milling. **b** Al7075-5 wt% SiC-5 wt% Gr after Ball milling. **c** Al7075-5 wt% SiC-10 wt% Gr after Ball milling. **d** Al7075-5 wt% SiC-0 wt% Gr after Sintering. **e** Al7075-5 wt% SiC-5 wt% Gr after Sintering. **f** Al7075-5 wt% SiC-10 wt% Gr after sintering



detailed microstructural characteristics of ball milled and sintered composites. All mixed powders are transformed from micro to nano size by performing ball milling operation. These powders are uniformly distributed throughout the Al 7075 matrix and can be seen from the SEM (ZEISS Supra 55VP) micrographs.

2.4 Wear Test

Dry sliding wear experiments have been carried out in conjunction with ASTM: G99-05 [32]. Evaluation standard on the pin-on-disk machine (Ducom, model No: ED-201, RCI DRDO, Hyderabad, India). EN31 steel is used as a counter disc material. Before experimentation, the pin shaped specimen and disk were cleansed with acetone (purity 99.50–99.99%) [33]. Every experiment was conducted on prepared hybrid- composite samples with loads ranging from 5 to 15 N. The selected range of sliding distances was about 1000–2000 m, including sliding speeds of 1 to 3 m per second for all the experiments. After each experiment, the counter and specimen surfaces were thoroughly cleansed using organic compounds to eliminate traces. To calculate

the amount of wear loss, the pin is measured before and after checking to a precision of 0.0001 g. The friction coefficient was calculated from obtained load values by strain-gauge [34]. All experiments were performed six times, and hence the responses from each run the average was registered in the table.

2.5 Design of Experiments

Taguchi's technique is a good tool for performing an investigation; it is quick, effective, and logical. When compared to standard techniques, this technique significantly reduces experimentation. However, the most significant disadvantage of this method is that it does not address the factors inter-relationships. A typical experiment requires one parameter at a time; all parameters must be kept fixed when one parameter is altered. Therefore, an investigation will be unable to analyse all variables to evaluate their significant effects (i.e. individual effects). Taguchi solves these issues. By using the Taguchi method, the problems that arise are all eliminated. In practical terms, the major outcome is reading responsive factors concerning certain levels. The total average reaction

is affected by the magnitude of its factor’s levels. The technique is designed for performance improvement and the determination of optimum factor-to-response formulations [35, 36]. These detailed testing results were carefully analysed and converted to produce a Signal/Noise ratio (S/N) as shown in Eq. (1). It has got different Signal/Noise ratios (S/N) exits for various properties. The minimum, maximum and nominal best are the three types of characteristics of S/N ratios included. Again, the minimal wear and frictional coefficients are beneficial.

AS SEEN BELOW, the S/N transformation is mathematically converted into a logarithmic model.

$$S/N = -10\log_{10} \left(\frac{1}{n} \sum y^2 \right), \tag{1}$$

For any ‘n’ data points, y represents the observed data.

Table 3 shows how the major four influencing parameters were examined in three stages. The tests were conducted subject to levels provided the tribological results in Table 4. The main effects plot was drafted with the Minitab-19 tool, while the contributing results were derived using ANOVA [37].

Table 3 Stages of factors information

Factors	Stage-I	Stage-II	Stage-III
A: Reinforcement (% of Gr.)	0	5	10
B: Load (N)	5	10	15
C: Sliding distance (m)	1000	1500	2000
D: Sliding speed (m/s)	1	2	3

3 Results and Discussion

3.1 Microstructure

The optical micrographs of the manufactured hybrid MMCs are shown in Fig. 2d–f. The optical microscopy

Table 4 Taguchi orthogonal array (L₂₇) design of experiments

S.No	Reinforcement (% of Gr.)	Load(N)	Sliding distance (m)	Sliding speed (m/s)	Wear loss (g)	SNRA1	COF	SNRA2
1	0	5	1000	1	0.0085	41.4116	0.1445	16.8026
2	0	5	1500	2	0.0098	40.1755	0.1643	15.6872
3	0	5	2000	3	0.0105	39.5762	0.1718	15.2995
4	0	10	1000	2	0.0096	40.3546	0.1812	14.8368
5	0	10	1500	3	0.0119	38.4891	0.1944	14.2261
6	0	10	2000	1	0.0203	33.8501	0.1528	16.3175
7	0	15	1000	3	0.0087	41.2096	0.2037	13.8202
8	0	15	1500	1	0.0145	36.7726	0.1801	14.8897
9	0	15	2000	2	0.0162	35.8097	0.1904	14.4067
10	5	5	1000	2	0.0037	48.6360	0.1489	16.5421
11	5	5	1500	3	0.0042	47.5350	0.1611	15.8581
12	5	5	2000	1	0.0133	37.5230	0.1356	17.3548
13	5	10	1000	3	0.0042	47.5350	0.1497	16.4956
14	5	10	1500	1	0.0112	39.0156	0.1421	16.9481
15	5	10	2000	2	0.0134	37.4579	0.1449	16.7786
16	5	15	1000	1	0.0067	43.4785	0.1863	14.5957
17	5	15	1500	2	0.0105	39.5762	0.1985	14.0448
18	5	15	2000	3	0.0121	38.3443	0.2032	13.8415
19	10	5	1000	3	0.0019	54.4249	0.1618	15.8204
20	10	5	1500	1	0.0103	39.7433	0.1561	16.1319
21	10	5	2000	2	0.0105	39.5762	0.1655	15.6240
22	10	10	1000	1	0.0075	42.4988	0.1702	15.3808
23	10	10	1500	2	0.0081	41.8303	0.1730	15.2391
24	10	10	2000	3	0.0129	37.7882	0.1758	15.0996
25	10	15	1000	2	0.0073	42.7335	0.1814	14.8273
26	10	15	1500	3	0.0109	39.2515	0.2011	13.9318
27	10	15	2000	1	0.0161	35.8635	0.2142	13.6806

findings demonstrated successful sample fabrication. The white region represents the Al7075 matrix in the optical microscope images, while the dark spots represent SiC and Graphite reinforcement particles. It is evident that the reinforcement particles in all samples are spread uniformly throughout the matrix material. Furthermore, the strong bonding between the matrix and the reinforcing structure appears to be excellent because the microstructures seen optically are essentially no porosity or non-existent in cracks. Prior research reports have shown that the homogeneous dispersion of the reinforcement in the matrix alloy is a critical element in obtaining better mechanical and tribological characteristics in the Al MMCs. Hence, achieving a homogeneous disbursement of reinforcement particles may promote better features in the investigated hybrid MMC samples.

Additionally, an SEM examination was conducted to analyze the more minute level of abnormalities, and the microstructures are represented in Fig. 3a–c. According to the SEM images, the manufactured hybrid MMC samples had little porosity and cracks on their surface, as seen in the image. Further, the pore sizes are incredibly tiny, measuring at about 1 μm , while the microcracks' length is around 10 μm . This level of difference is remarkably negligible. The microscopic examination thus finds that a homogeneous reinforcement dispersion and robust interfacial bonds between particles and matrix are formulated, contributing to excellent friction and wear characteristics.

3.2 Density and Hardness

Figures 4 and 5. the plotted results revealed that the hybrid composites' density and hardness decrease as the graphite reinforcement's weight percentage increases. This is due to its low density and soft content increases as the graphite percentage increases. By varying Graphite and keeping the SiC constant, the mechanical properties and tribological properties are optimized.

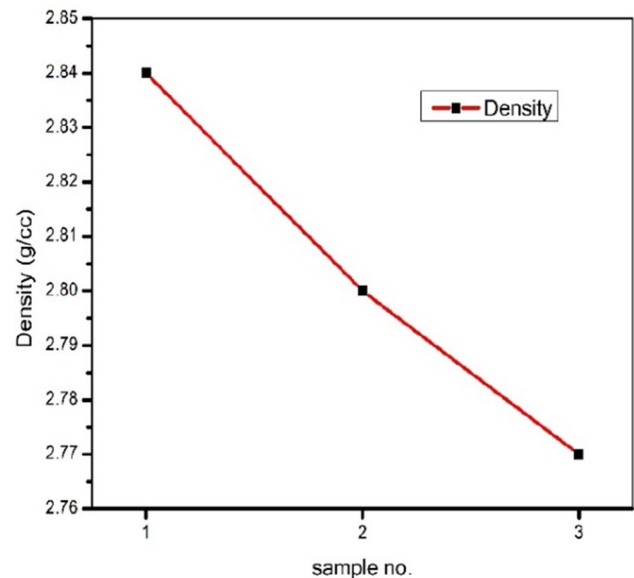
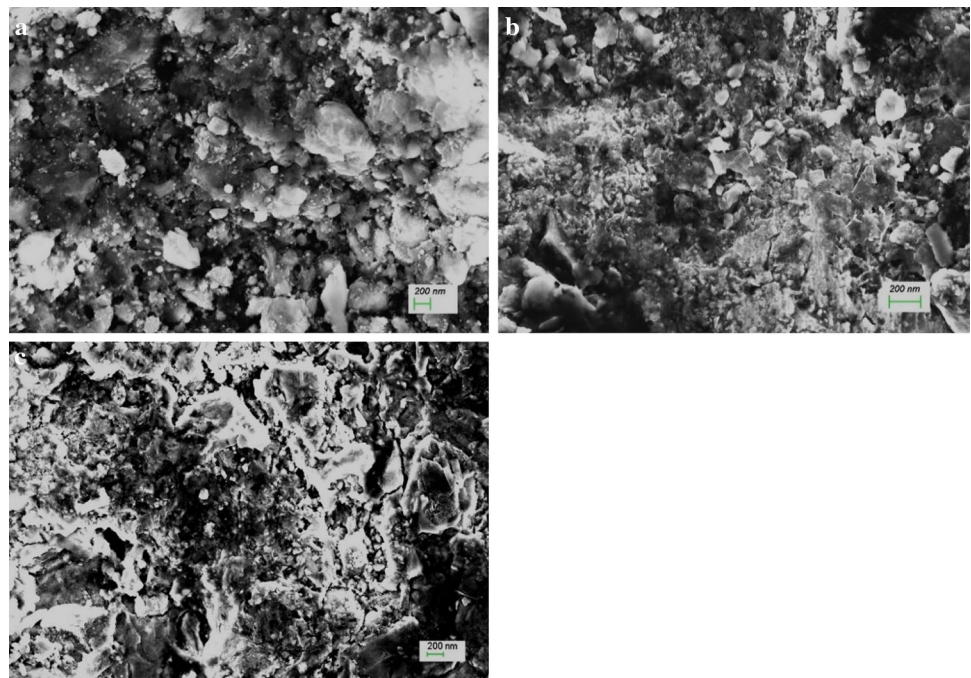


Fig. 4 The density of Hybrid-composites

Fig. 3 a Al7075-5 wt.% SiC-0 wt.% Gr after Sintering. b Al7075-5 wt.% SiC-5 wt.% Gr after sintering. c Al7075-5 wt.% SiC-10 wt.% Gr after sintering



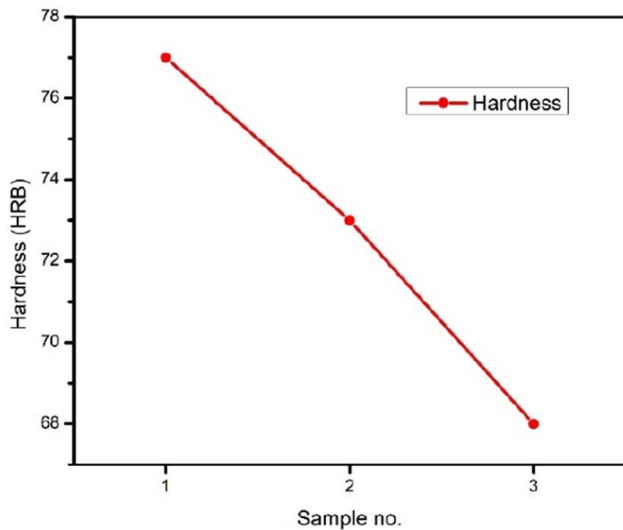


Fig. 5 The hardness of Hybrid-composites

3.3 ANOVA and Significant Influence of Parameters for Wear

As for the other factors, A (Reinforcement (% of Gr.)), B (Load, N), C (Sliding Distance, m) and D (Sliding Speed, m/s), it was beneficial to create an ANOVA table to show their combined effects. This analysis was done for a confidence level of significance of 5%. Tables 5 and 6 present the overall findings of the investigation in terms of examining the wear and friction coefficients. Table 5 Sliding distance ($p = 55.98\%$ of the distance travelled) significantly influenced wear loss. Load ($p = 13.31\%$), sliding velocity ($p = 11.36\%$), and reinforcing weight percentage ($p = 13.31\%$) all reduced the wear loss, but the interrelationships have not significantly contributed to the wear loss.

Similarly, Table 6 shows that the load contributed significantly to the coefficient of friction ($p = 61.25\%$). On the other hand, friction coefficient ($p = 8.7\%$) contribution to Graphite reinforcing weight percentage and sliding velocity

Table 5 ANOVA for wear loss

Source	DF	Adj SS	Adj MS	F Value	P Value	Contribution (%)
Reinforcement (wt. % of Gr)	2	0.000059	0.000030	22.55	0.000	13.31
Load (N)	2	0.000059	0.000030	22.65	0.000	13.31
Sliding distance (m)	2	0.000248	0.000124	94.57	0.000	55.98
Sliding velocity (m/s)	2	0.000053	0.000027	20.33	0.000	11.96
Error	18	0.000024	0.000001			5.41
Total	26	0.000443				

S = 0.0011448, R-Sq = 94.68% and R-Sq (adj) = 92.31%

Table 6 ANOVA for friction coefficient

Source	DF	Adj SS	Adj MS	F value	P value	Contribution (%)
Reinforcement (wt. % of Gr)	2	0.001023	0.000511	4.17	0.033	8.7
Load (N)	2	0.007192	0.003596	29.32	0.000	61.25
Sliding distance (m)	2	0.000103	0.000052	0.42	0.663	0.87
Sliding velocity (m/s)	2	0.001215	0.000608	4.95	0.019	10.35
Error	18	0.002208	0.000123			18
Total	26	0.011741				

S = 0.0011448, R-Sq = 94.68% and R-Sq (adj) = 92.31%

Fig. 6 Main effects plot of factors for Wear loss of Al7075 composites

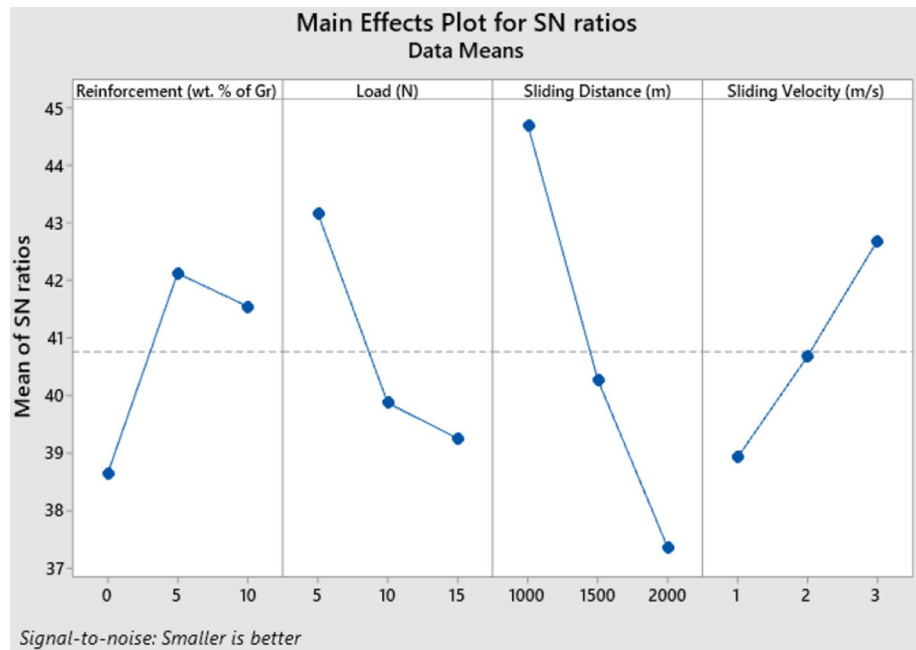
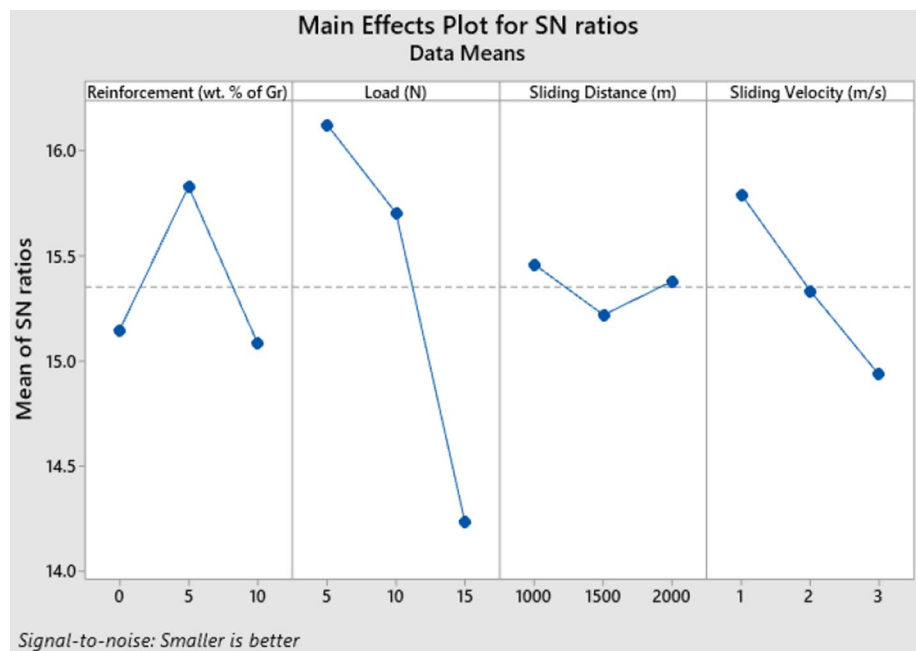


Fig. 7 Main effects plot of factors for the friction coefficient of Al7075 composites

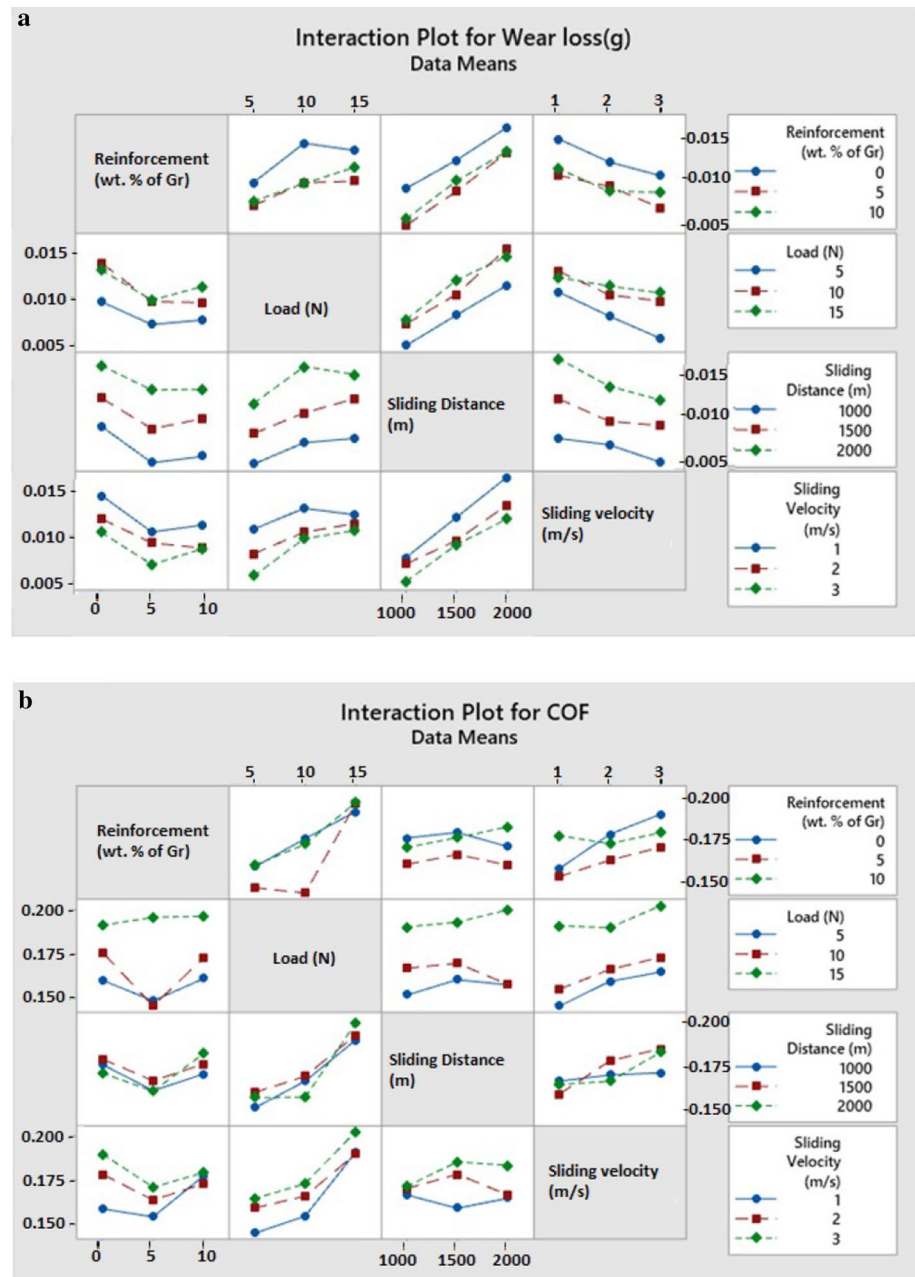


was less significant ($p = 10.35\%$). Here, the error value percentage shows that the interrelationships less significantly contribute to the coefficient of friction. Hence, this study showed that wear loss is influenced substantially by the sliding distance. Furthermore, the load was the most significant factor in influencing the friction coefficient. The Graphite percentage (13.31 and 8.7%) seemed to benefit from both instances.

3.4 Effects of Experimental Parameters on Wear

Figures 6 and 7 illustrate the major effects of the different experimental parameters on the tribological properties of composites. There is no major influence within that main effect graph when the reading for a certain parameter is close to horizontal. In comparison, the most obvious impact is a parameter for the line with the greatest slope. The main effect graph shows that only parameter C (sliding distance) was the strongest effect, whereas the others (load, speed,

Fig. 8 a, b Interaction plots.
a Interaction plot for wear loss (g).
b interaction plot for coefficient of friction (μ)



and reinforcement percentage) were less influential. The improvement in the sliding distance resulted in more contact time between asperity to asperity and an improved actual contact field, which in turn contributed to wear formation and increasing wear on composites. Wear loss was improved by increasing the load and sliding distance, indicating that the material is detached more from the specimen base [38].

Furthermore, wear is reduced because of the formation of a thick tribo crust of Graphite on the worn base. Therefore, wear is reduced by incorporating additional contact areas. The 5% hybrid composite showed significantly greater wear performance at all parameters than others (i.e., 0 percent and 10 percent).

3.5 Effect of Various Designed Test Parameters on the Friction Coefficient

Figure 8a, b illustrates the effect of the test conditions on the friction coefficient. Applied load (as criterion B) had the most significant influence on friction coefficient, whereas the other test parameters, sliding speed and percentage of Graphite, had only comparatively small implications. The friction remains practically invariant with sliding distance amongst all composite materials. The rise in the load considerably raised the friction coefficient of the composites, so the graphite layer was more durable at smaller loads than at greater loads because the graphite layer was eroded more

Table 7 Wear loss S/N ratio response table: smaller the better

Level	Reinforcement (wt. % of Gr)	Load (N)	Sliding distance (m)	Sliding velocity (m/s)
1	38.63	43.18	44.70	38.91
2	42.12	39.87	40.27	40.68
3	41.52	39.23	37.31	42.68
Delta	3.49	3.95	7.39	3.78
Rank	4	2	1	3

Table 8 Coefficient of friction S/N ratio response table: smaller the better

Level	Reinforcement (wt. % of Gr)	Load (N)	Sliding distance (m)	Sliding velocity (m/s)
1	15.14	16.12	15.46	15.79
2	15.83	15.70	15.22	15.33
3	15.08	14.23	15.38	14.93
Delta	0.75	1.90	0.24	0.86
Rank	3	1	4	2

rapidly when the load increased. As the weight percentage continuously adds up to a certain percentage of Graphite (5%), the coefficient of friction decreases; after that, it increases as the weight percentage of graphite increases. This effect is attributable to the addition of Graphite to the Al7075 matrix, which serves as a strong lubricant and causes a layer of the lubricant-rich substrate to build on the tribo-surface, hence minimizing friction. When Graphite's weight percentage exceeded 5%, friction exhibits a steady increase in wear because of an increase in the number of cracks in the oxide layer found on the surface, which degrades worn surfaces. Abrasion occurs when sliding surfaces abrade one other. It could result in composite adhesion to the counter face. Therefore, adhesion continued to rise, leading to a corresponding rise in the coefficient of friction.

Table 9 Details of confirmation experiment

Level	Initial factor settings	Optimal factor settings	
		Predicted results	Actual testing results
	A3B3C3D3	A2B1C1D3	
Wear loss (g)	0.0137	0.0014	0.0013
S/N ratio in dB	37.2656	57.0774	57.7211
Percentage of improvement in S/N Ratio	20.45		
	A3B3C3D3	A2B1C1D1	
Coefficient of friction	0.218	0.1374	0.1349
S/N ratio in dB	13.2309	17.1469	17.3998
Percentage of improvement in S/N ratio	4.17		

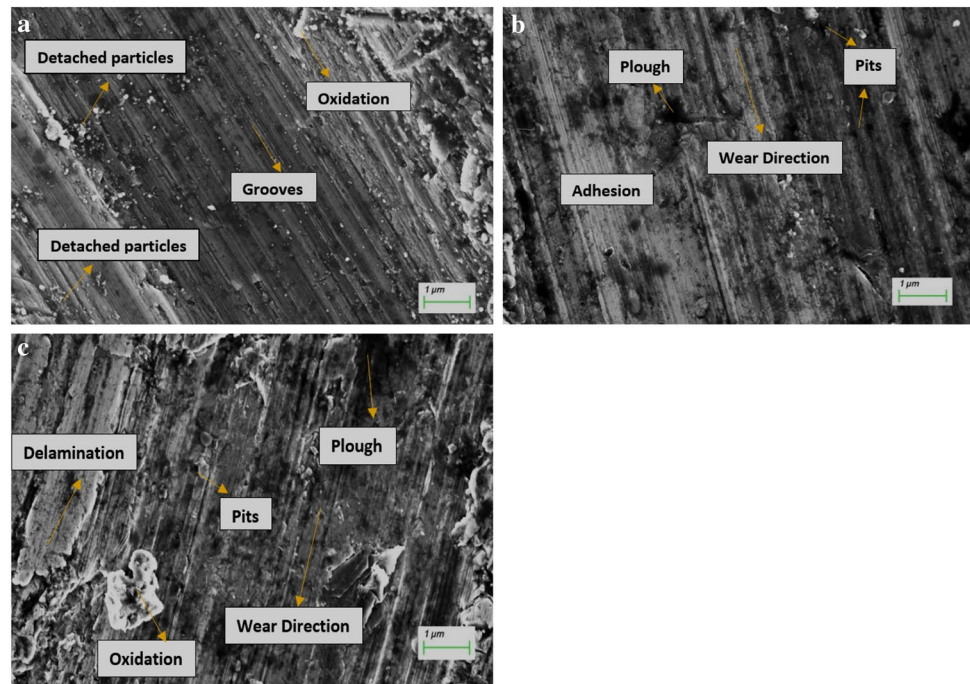
3.6 Experimental Analysis and Validation Utilising the Taguchi Technique

Signal-to-noise ratio (S/N) is the primary criteria for analysis in the Taguchi technique. The Taguchi technique recommends a maximum S/N ratio to achieve optimal testing parameters in this research. Tables 7 and 8 show the S/N responses data for the wear properties of the developed composites. The response table represents almost every level of the parameters. The response table lists rankings as per delta statistic values, which checks out the magnitude of impacts. The delta statistic is measured by the difference between the largest and smallest averages for each parameter in statistical terms. Thus, when assigning ranks, the highest delta value will be awarded the rank of 1, the second largest will be 2, and so on [35]. The optimal parameter settings that offered the best results were a Graphite reinforcement of 5 percent, a load of 5 N, a sliding distance of 1000 m, and a sliding velocity of 3 m/s for best wear loss. Moreover, a Graphite reinforcement of 5 percent and loads of 5 N and sliding distances of 1000 m, and speeds of 1 m/s for friction coefficient.

3.7 Experiment for Confirmation

It is strongly recommended to conduct a reliability and validity experiment to verify the experimental findings. After identifying the ideal parameters, the confirmation experiment was conducted to validate the predicted performance, as shown in Table 9. Comparative analysis of wear loss estimated with actual wear loss using optimal parameters shown in Table 9 [35]. When comparing predicted and actual outcomes, it should be noted that there is a high degree of close agreement. The S/N ratio of the original test settings to the optimum testing conditions has increased by 20.45 dB and 4.17 dB, which reduces wear loss by around 45.11 percent and the friction coefficient by 68.50 percent. The results confirmed that the model developed in this research work could effectively estimate the tribological properties.

Fig. 9 a–c SEM micrographs of hybrid composites. **a** Al 7075-5 wt% SiC -0 wt% Gr at load 5N, SD 1000 m, SV 1 m/s. **b** Al 7075-5 wt% SiC -5 wt% Gr at load 5N, SD 1000 m, SV 1 m/s. **c** Al 7075-5 wt% SiC -10 wt% Gr at load 5N, SD 1000 m, SV 1 m/s



Regression equation
for Wear loss (g)

$$\begin{aligned} \text{wearloss(g)} = & 0.00043 - 0.000272\text{Reinforcement(wt.\%ogGr)} \\ & + 0.000337\text{Load(N)} + 0.000007\text{Sliding distance(m)} \\ & - 0.001728\text{Sliding Velocity}\left(\frac{\text{m}}{\text{s}}\right), \end{aligned} \quad (2)$$

for coefficient of friction

$$\begin{aligned} \text{COF} = & 0.1126 + 0.000177\text{Reinforcement(wt.\%ogGr)} \\ & + 0.003881\text{Load(N)} + 0.000003\text{Sliding Distance(m)} \\ & + 0.00782\text{Sliding Velocity}\left(\frac{\text{m}}{\text{s}}\right) \end{aligned} \quad (3)$$

3.8 Wear Mechanism

SEM examinations of the worn-out surfaces shown in Fig. 9a–c. The standard SEM images of sintered samples for the Al7075–5wt.% SiC composite morphologies shown in Fig. 9a indicate the Al7075–5wt.% SiC composite's wear behaviour shows the wear produced by deeper stable strips and the breakage of its oxide film, thereby resulting rise in wear loss. It demonstrates that Al7075–5wt.% SiC was subjected to considerable significant plastic deformation, resulting in fractured SiC reinforcements. These composites (Fig. 9b and c) have more good patterns and mild plastic deformation at their groove boundaries. These graphite reinforcements provide more smoothness to the substrate surface. Figure 9c illustrates the microstructure of the

Al7075–5wt.% SiC–10wt.% Gr hybrid, which shows significant wear characteristics.

Graphite particles dispersed throughout the aluminum matrix, which helped to reduce the wear particles mean size. Conversely, the hybrid composite wear debris mixed coarse and fine particles with non-uniform patterns. As demonstrated, 10 wt.% graphite composites had longer strips of debris than 5 wt.% graphite composites, as the fracture of reinforcing particles were predominant over the solid lubricant effect. The mechanism was characterized as forming a series of deep grooves due to ploughing action, worn debris hardens, and asperities scratch deeply into composites counter discs [17, 40–43].

The increasing temperature of the sliding surfaces during wear-testing is a significant determinant of the wear mechanism [44–47]. From Fig. 8, it can be observed that the temperature on worn-out surfaces of Al7075–5wt.% SiC and the Al7075–5wt.% SiC–10wt.% Gr composites more rapidly increasing than the temperature on the Al7075–5 wt.% SiC–5wt.% Gr composites, this is due to the higher coefficient of friction at the surface of both the Al7075–5wt.% SiC and the Al7075–5wt.% SiC–10wt.% Gr composites with respect to counterpart. This Al7075–5wt.% SiC–5wt.% Gr composites exhibited reduced friction co-efficient than the Al7075–5wt.% SiC–10wt.% Gr composite (refer Table 5). These characteristics slow down the increase of temperature increase during the wear process, which reduces the composite's interface adhesiveness [44]. Moreover, the wear characteristics of the worn-out surface were reduced due to improved graphite self-lubrication.

Figure 9c illustrates the substrate surface film upon its worn-out surfaces of the Al7075–5wt.% SiC–10wt.%Gr and Al–5wt.%SiC– 5wt.%Gr hybrid composites was shown in Fig. 9b. Figure 9c shows the loose particles at the work surface, mainly aluminum matrix oxide particles, demonstrating the worn-out surface's severe deformation. Whereas in Fig. 9b, it was observed that graphite microparticles, with tiny, oxidized particles present at the worn-out area. Furthermore, this ensures that small particulates are well-packed together and generated an adhesive layer across

the surfaces. As a result, pin surface deformation due to plasticity was significantly reduced in the Al7075–5wt.% SiC–5wt.% Gr hybrid composite. Because of this, its temperature rise was decreased. This way, soft graphite particles combine with retained loose debris and form a graphite rich tribo-layer on the work surface. Thus, the excessive wear will be reduced in Al7075–5wt.% SiC–5wt.% Gr combinations and abrasion, delamination are the predominant sources of wear [45, 46].

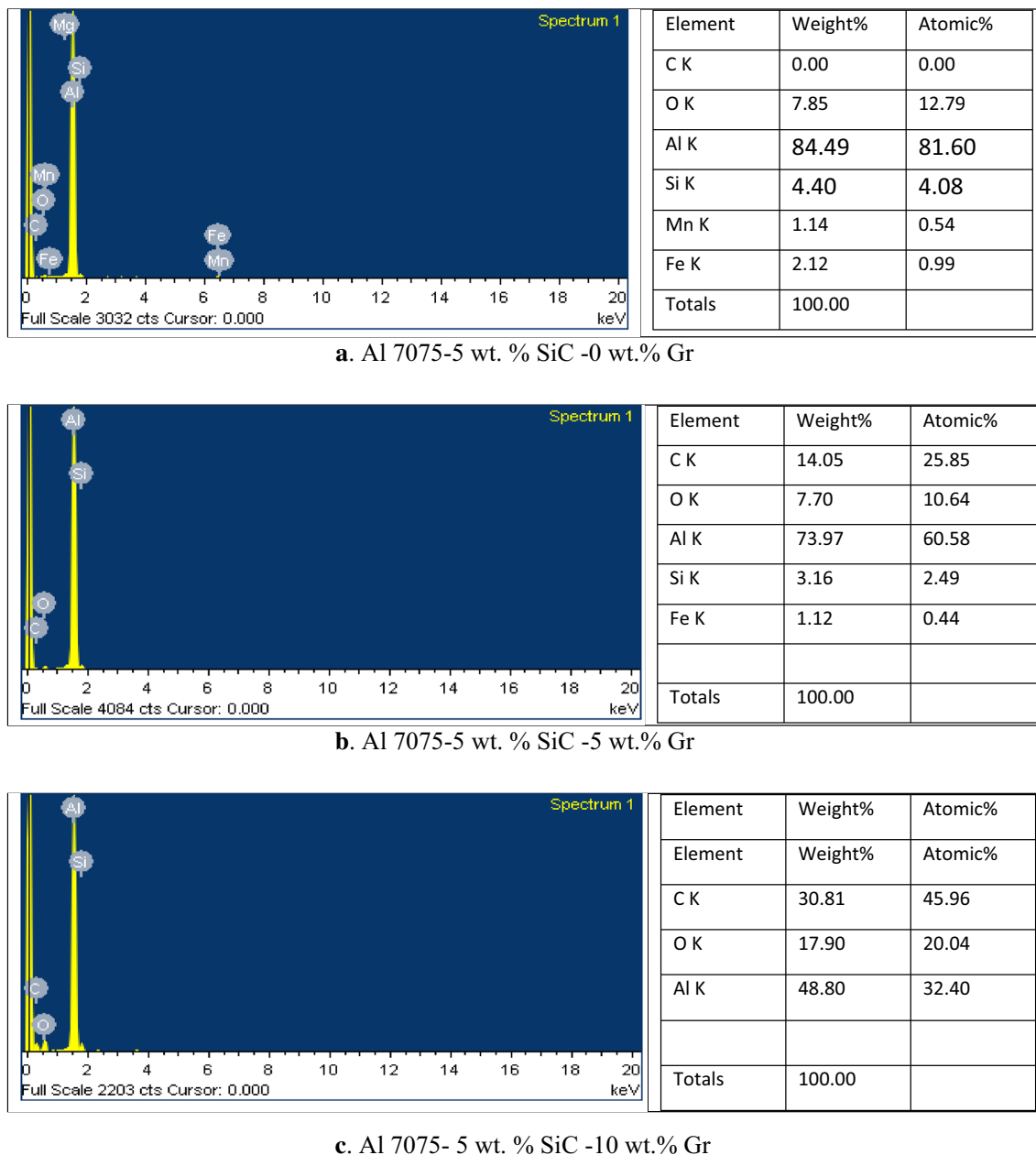


Fig. 10 a–c EDX spectrum of worn surfaces **a** Al7075–5% SiC composite. **b** Al7075–5% SiC–10% Gr composite and **c** Al7075–5% SiC–5% Gr composite

3.9 EDX Analysis

According to the dry wear settings, energy dispersed X-rays (EDX) testing of worn-out composite surfaces was carried out. The EDX findings for hybrid composites showed that minor level oxygen peaks were observed in all cases, indicating that a small amount of oxidation has formed on the worn-out surfaces. This can be due to the presence of oxidation on the worn-out surfaces. The slip at the interface of composite pin and steel countertop (EN31) increases temperature and the ambient air reactions, this may form an oxidation layer at the interface [47, 48]. The EDX profile results of Al7075-5wt%SiC composite were shown in Fig. 10a. The higher peaks of Al in Fig. 10a can be interpreted as the plastic deformation on Al7075-5 wt. % SiC composite. Al7075-5wt.% SiC-10% Gr hybrid composite, clear carbon peaks can be seen compared to the EDX profile of the Al7075-5wt.% SiC composites. Figure 10c shows the EDX profile of a worn-out surface of an Al7075-5wt.% SiC-10% Gr hybrid composite. In Fig. 10a, clear carbon peaks can be seen compared to the EDX profile of the Al7075-5 wt% SiC composites worn-out surface.

The minimum intensity of the Carbon(C) peak shows graphite inefficiency on sliding surfaces without developing any graphite layer. The significant level of the Si pattern shows that SiC particulates have been drawn from the Al7075 matrix. Figure 10b shows the EDX profile of the worn-out surfaces of the Al7075-5wt% SiC-5wt% Gr hybrid composite. The high C peak verified the improved dispersion of graphite particulates at the contact surface and the low intensity of the Al peak compared to the other two EDX measurements. Furthermore, the addition of the SiC particulates caused the steel countertop to scratch, which allowed the appearance of a significant Ferrous (Fe) peak. The existence of a low oxygen peak has been detected in all composites EDX findings. This peak showed oxide development on the worn-out surface of the sliding components.

4 Conclusion

In this research study, the powder metallurgical technique produced Al7075/SiC/Graphite hybrid composites accurately and efficiently. The hardness and density of hybrid composites are reduced because Graphite's weight percentage (i.e., 0 percent and 10 percent) has increased. The hybrid composites containing a weight percentage of 5% of Graphite demonstrated superior wear and tribological properties. Incorporating graphite particles as secondary reinforcements into the aluminum 7075 matrix significantly improves tribological characteristics.

The ANOVA findings revealed that wear loss is affected by factors such as the sliding distance (55.98%), sliding

speed (11.96%), applied force (13.31%), and the weight percentage of Graphite in the composite (13.31%), for the specified experiments. The critical factors influencing the coefficient of friction of the composites were the applied load (61.25%), sliding distance (0.87%), sliding speed (10.35%), and the graphite reinforcement (8.7%). In a Taguchi observational investigation, the optimized process parameters for wear loss and coefficient of friction were determined to be A2B1C1D3 and A2B1C1D1, respectively. As a result, the S/N ratio of the original test settings to the optimum testing conditions has increased by 20.45 dB and 4.17 dB, which reduces wear loss by around 45.11 percent and the friction coefficient by 68.50 percent.

Funding This research received no specific grant from any funding agency.

Data Availability This manuscript has no associated data.

Declarations

Conflict of interest The authors declare that they have no known competing financial interests or personal relationships that could have appeared to influence the work reported in this paper. No Potential conflict of interest was reported by the authors.

References

1. Chipise L, Jain PK, Cornish LA (2021) Sliding wear characteristics of WC-VC-Co alloys with various Ru additions. *Int J Refract Metal Hard Mater* 95:105429
2. Průša F, Vojtěch D, Bláhová M, Michalcová A, Kubatík TF, Čížek J (2015) Structure and mechanical properties of Al-Si-Fe alloys prepared by short-term mechanical alloying and spark plasma sintering. *Mater Design* 75:65–75
3. Wu Q, Xu W, Zhang L (2019) Machining of particulate-reinforced metal matrix composites: an investigation into the chip formation and subsurface damage. *J Mater Process Technol* 274:116315
4. Wu Q, Xu W, Zhang L (2021) Advances in the machining of particulate-reinforced metal matrix composites. *Adv Mach Finish* 45–75
5. Fenghong C, Chang C, Zhenyu W, Muthuramalingam T, Anbuezhhiyan G (2019) Effects of silicon carbide and tungsten carbide in aluminium metal matrix composites. *SILICON* 11(6):2625–2632
6. Sridhar A, Lakshmi KP (2021) Evaluation of mechanical and wear properties of aluminum 7075 alloy hybrid nanocomposites with the additions of SiC/Graphite. *Mater Today Proceed* 44:2653–2657
7. Khan M, Rehman A, Aziz T, Shahzad M, Naveed K, Subhani T (2018) Effect of inter-cavity spacing in friction stir processed Al 5083 composites containing carbon nanotubes and boron carbide particles. *J Mater Process Technol* 253:72–85
8. Zakaulla M, Arjun R, Khan MA, Khan IH, Pasha N (2018) Tribological characteristics of multiwalled carbon nanotubes and boron carbide particles reinforced Al2024 matrix composites. *Mater Today Proc* 5762–5767

9. Sharma H, Tiwari SK, Chauhan VS, Kumar R, Gulati P (2021) Wear analysis of friction stir processed aluminum composite reinforced by boron carbide. *Mater Today Proc*
10. Balaji D, Vetrivel M, Ekambaram M, Vijayaraghavan S, Gowtham KD (2018) Tribological behaviour on aluminium–nano Titanium Di Oxide with addition of solid lubricant nano Gr powder metallurgy composite. *IOP Conf Series Mater Sci Eng* 390(1):012030
11. Nieto A et al (2017) Reinforcement size effects on the abrasive wear of boron carbide reinforced aluminum composites. *Wear* 390–391:228–235. <https://doi.org/10.1016/j.wear.2017.08.002>
12. Alaneme KK et al (2019) Development of aluminum-based composites reinforced with steel and graphite particles: structural, mechanical and wear characterization. *J Mater Res Technol* 8(1): 670–682
13. Bhoi NK, Singh H, Pratap S (2019) Developments in the aluminum metal matrix composites reinforced by micro/nano particles: a review. *J Comp Mater*. <https://doi.org/10.1177/0021998319865307>
14. Elkady OA, Yehia HM, Ibrahim AA, Elhabak AM, Elsayed EM, Mahdy AA (2021) Direct observation of induced graphene and SiC strengthening in Al-Ni alloy via the hot pressing technique. *Crystals* 11(9):1142. <https://doi.org/10.3390/CRYST11091142>
15. Wang K, Zhang ZM, Yu T, He NJ, Zhu ZZ (2017) The transfer behavior in centrifugal casting of SiCp/Al composites. *J Mater Process Technol* 242:60–67
16. Gürçan K, Derin B, Erhan AYAS. Effect of SiC particle size on the microstructural, mechanical and oxidation properties of in-situ synthesized HfB₂-SiC composites. *Politeknik Dergisi* 1–1
17. Rao TB (2018) An experimental investigation on mechanical and wear properties of Al7075/SiCp composites: effect of SiC content and particle size. *J Tribol* 40(3)
18. Włodarczyk-Fligier A, Dyzia M, Polok-Rubiniec M (2015) TEM investigations of aluminium composite materials reinforced with Ti (C, N) ceramic particles. *Solid State Phenom* 229:57–62
19. Bharti C, Singh A, Rahul R, Sharma D, Dwivedi SP (2021) A critical review of aluminium based composite developed by various casting technique with different reinforcement particles to enhance tribo-mechanical behaviour. *Mater Today Proceed*
20. Asha PB, Murthy SS, Suresha CN (2021) Investigation of physical, mechanical and wear behavior of aluminium composite carrying ceramic Boron carbide particles. *Mater Today Proceed*
21. Mironov A, Gershman I, Gershman E, Podrabinnik P, Kuznetsova E, Peretyagin P, Peretyagin N (2021) Properties of journal bearing materials that determine their wear resistance on the example of aluminum-based alloys. *Materials* 14(3):535
22. Zeren A (2015) Effect of the graphite content on the tribological properties of hybrid Al/SiC/Gr composites processed by powder metallurgy. *Indus Lubric Tribol*
23. Kumar VN, Kishore Nath N, Ramesh Babu P (2020) Effect of reinforcement and fabrication of Al6061 nanosilica composite prepared using single-and two-step methods. *Adv Mater Process Technol* 1–20
24. Jurwall V, Sharma AK, Pandey A (2020) Fabrication characterisation and machining of micro hybrid Al6061 aluminium composite. *AIP Conf Proc* 2273(1):030006
25. Atla S, Kaujala PL (2020) Investigation of graphite effect on the mechanical and tribological properties of Al 7075-SiC-graphite hybrid metal matrix composites. *Tribologia-Finnish J Tribol* 37(1–2):26–32
26. Kandagal ZB, Akkimardi VG, Sonnad AN (2021) Investigation on microstructural and mechanical properties of microwave welded Al6061-SiC-graphite hybrid metal matrix composites. *Metallogr Microstruct Anal* 1–13
27. Sharath BN, Jeevan TP, Baig MAA, Ashrith HS, Afzal A, Reddy AR (2021) Machinability studies on boron carbide and graphite reinforced aluminium hybrid composites. *Mater Today Proc*
28. Wieczorek J, Dyzia M, Dolata AJ (2012) Machinability of aluminium matrix composites. *Solid State Phenom* 191:75–80
29. Krishnamurthy L, Sridhara BK, Budan DA (2007) Comparative study on the machinability aspects of aluminium silicon carbide and aluminium graphite composites. *Mater Manuf Processes* 22(7–8):903–908
30. Ritapure PP, Kharde YR (2020) Study of Mechanical properties and erosion wear behaviour of novel Al-25Zn alloy/SiC/Graphite hybrid composites. *Mater Today Proc* 22:2215–2224
31. Pournaderi S, Akhlaghi F (2017) Wear behaviour of Al6061-Al2O₃ composites produced by in-situ powder metallurgy (IPM). *Powder Technol* 313:184–190
32. ASTM G99–95 (1995) Standard test method for wear testing with a pin-on-disk apparatus. *Am Soc Testing Mater*
33. Straffellini G (2015) Friction and wear. *Methodologies for Design and Control*. Springer International Publishing AG Switzerland, Switzerland
34. Singh MK, Gautam RK (2019) Dry sliding friction and wear behaviour of developed copper metal matrix hybrid composites. *Int J Surf Sci Eng* 13(2–3):133–155
35. Myers RH, Montgomery DC, Anderson-Cook CM (2016) Response surface methodology: process and product optimisation using designed experiments. John Wiley and Sons, USA
36. Panja B, Das SK, Sahoo P (2015) Tribological behaviour of electroless Ni–P coatings in brine solution and optimisation of coating parameters using Taguchi based grey relation analysis. *J Instit Eng* 96(3):299–309
37. Kenett RS, Zacks S (2021) Modern industrial statistics: with applications in R, MINITAB, and JMP. John Wiley and Sons, USA
38. Venkatesh VSS, Deoghare AB (2021) Microstructural characterisation and mechanical behaviour of SiC and kaoline reinforced aluminium metal matrix composites fabricated through powder metallurgy technique. *Silicon*, 1–15
39. Raj R, Thakur DG (2018) Influence of boron carbide content on the microstructure, tensile strength and fracture behavior of boron carbide reinforced aluminum metal matrix composites: Einfluss des Borkarbidgehaltes auf Gefüge, Zugfestigkeit und Bruchverhalten von Borkarbid verstärkten Metallmatrix-Verbundwerkstoffen. *Materialwiss Werkstofftech* 49(9):1068–1080
40. Ravindran P, Manisekar K, Narayanasamy R, Narayanasamy P (2013) Tribological behaviour of powder metallurgy-processed aluminium hybrid composites with the addition of graphite solid lubricant. *Ceram Int* 39(2):1169–1182
41. Hu CJ, Yan HG, Chen JH, Bin SU (2016) Microstructures and mechanical properties of 2024Al/Gr/SiC hybrid composites fabricated by vacuum hot pressing. *Trans Nonferrous Metals Soc China* 26(5):1259–1268
42. Lee H (2019) Generation of airborne wear particles from wheel–rail contact during rolling/sliding and pure sliding contact. *Wear* 426:1797–1806
43. Feng K, Shao T (2021) The evolution mechanism of tribo-oxide layer during high temperature dry sliding wear for nickel-based superalloy. *Wear* 203747
44. Altinkök N (2013) Mechanical properties and wear behaviour of Al2O₃/SiCp reinforced aluminium-based MMCs produced by the stir casting technique. *Adv Comp Lett* 22(4)
45. Jin K, Qiao Z, Zhu S, Cheng J, Yin B, Yang J (2016) Friction and wear properties and mechanism of bronze–Cr–Ag composites under dry-sliding conditions. *Tribol Int* 96:132–140

46. Gautam RK, Sharma SC, Jain SC, Ray S (2013) Dry sliding wear behavior of hot forged and annealed Cu-Cr-SiC in situ composite. *Mater Sci Forum* 736:207–217
47. Rajkumar K, Aravindan S (2011) Tribological performance of microwave sintered copper–TiC–graphite hybrid composites. *Tribol Int* 44(4):347–358
48. Konieczny M (2020) Processing and properties of sintered copper-iron and copper-steel composites, metal Conference Proceedings. <https://doi.org/10.37904/metal.2020.3579>

Publisher's Note Springer Nature remains neutral with regard to jurisdictional claims in published maps and institutional affiliations.